Uncertainties in determining parton distributions at large x

A. Accardi

Hampton University, Hampton, Virginia 23668 and

Jefferson Lab, Newport News, Virginia 23606

W. Melnitchouk

Jefferson Lab, Newport News, Virginia 23606

J. F. Owens

Florida State University, Tallahassee, Florida 32306

M. E. Christy, C. E. Keppel, L. Zhu

Hampton University, Hampton, Virginia 23668

J. G. Morfín

Fermilab, Batavia, Illinois 60510

Abstract

We critically examine uncertainties in parton distribution functions (PDFs) at large x arising from nuclear effects in deuterium F_2 structure function data. Within a global PDF analysis, we assess the impact on the PDFs from uncertainties in the deuteron wave function at short distances and nucleon off-shell effects, from the use of relativistic kinematics, and from the use of less a restrictive parametrization of the d/u ratio. We find in particular that the d-quark and gluon PDFs vary significantly with the choice of nuclear model. We highlight the impact of these uncertainties on the determination of the neutron structure functions, and on W boson production and parton luminosity at the Tevatron and the LHC. Finally, we discuss prospects for new measurements sensitive to the d-quark and gluon distributions but insensitive to nuclear corrections.

I. INTRODUCTION

Parton distribution functions (PDFs) are traditionally determined *via* global fits to a wide variety of data for large momentum transfer processes [1–7]. Typical data sets include deep inelastic scattering (DIS) of charged leptons on proton and deuterium targets or neutrinos on heavy nuclear targets, lepton pair production on proton and deuterium targets, and the production of photons, vector bosons, or jets at large values of transverse momentum. The use of deuterium targets in charged lepton DIS and heavy nuclear targets for neutrino DIS brings in the added complication of having to account for the modifications of the PDFs in a nuclear environment compared to the PDFs of free nucleons.

One of the key goals of such global fits is the determination of the flavor dependence of the extracted PDFs, *i.e.*, determining the PDFs for each parton flavor separately. The classic method for disentangling the u and d PDFs is to compare charged lepton DIS on proton and deuterium targets. In order to concentrate on the extraction of the leading twist PDFs, cuts specifying minimum values of Q^2 and W^2 are usually employed, thereby reducing the contributions of higher twist terms and target mass corrections. The effect of these cuts is to restrict the range in x to the region $x \lesssim 0.7$. In this region it is usually assumed that deuterium nuclear corrections are a few per cent or less and are, therefore, negligible. Accordingly, most global fits ignore deuterium nuclear corrections.

In our previous analysis [1] the effects of systematically reducing the cuts on Q^2 and W^2 were studied. This opened up the possibility of including data at larger values of x than those typically used in global analyses. Target mass effects were included along with a parametrization of higher twist terms. It was found that the leading twist PDFs were stable to variations in the techniques used to calculate the target mass corrections, provided that a sufficiently flexible higher twist parametrization was employed. However, it was observed that the d PDF was particularly sensitive to the assumptions used to calculate the nuclear corrections in deuterium. The purpose of the study reported here is to further investigate and quantify the effects of nuclear corrections on PDFs in global fits which make use of data obtained with deuterium targets, and to assess their impact on the neutron structure function determination, as well as on W production and parton luminosities at the Tevatron and the Large Hadron Collider (LHC).

In Section II we present a detailed discussion of the nuclear corrections which must be

accounted for when using deuterium targets, including those arising from the conventional nuclear Fermi motion and binding, nucleon off-shell and relativistic effects, and nuclear shadowing at small x. Section III contains a brief summary of the data used, along with the fitting procedures, and a detailed discussion of the flavor dependence of the various observables considered in this study, with particular emphasis on the large-x region. Section IV discusses the results of our fits, which we refer to as "CJ" (CTEQ-Jefferson Lab) fits. Future experimental possibilities to reduce the uncertainty in the d-quark and gluon PDFs are outlined in Sec. V, and our conclusions are summarized in Sec. VI.

II. NUCLEAR EFFECTS IN DEUTERIUM

Because the deuteron is a weakly bound nucleus, most analyses have assumed that it can be treated as a sum of a free proton and neutron. On the other hand, it has long been known from experiments on nuclei that a nontrivial x dependence exists for ratios of nuclear to deuterium structure functions. While the ratio of the deuteron to isoscalar nucleon structure functions has yet to be measured directly due to the absence of free neutron targets, most theoretical studies suggest the presence of non-negligible nuclear effects also in deuterium, although at a level smaller than for heavy nuclei due to the deuteron's small binding energy, $\varepsilon_d = -2.2$ MeV. Particularly in the region $x \gtrsim 0.5$ the effects of nuclear Fermi motion lead to a rapidly increasing ratio of deuteron to nucleon structure functions, $R^{d/N} \equiv F_2^d/F_2^N$, which diverges as $x \to 1$. Any high-precision analysis of the large-x region must therefore account for the nuclear effects if data on deuterium (or other nuclei) are used in the fit.

In this section we first review the standard nuclear corrections in the deuteron, including the effects of nucleon Fermi motion and binding, formulated within the framework of the weak binding approximation (WBA) [8–10]. For most kinematics of relevance to global PDF analyses a nonrelativistic description of the deuteron is sufficient; however, at large values of x ($x \gtrsim 0.7$) the effects of relativity become increasingly important. We therefore explore the sensitivity of the nuclear corrections to relativistic kinematics, as well as to the short-distance nucleon–nucleon (NN) interaction parametrized through different nonrelativistic and relativistic deuteron wave functions. Finally, the dependence of the structure function of the bound nucleon on its virtuality is explored within several models and phenomeno-

3

logical parametrizations and its impact on the $R^{d/N}$ ratio assessed. Although not affecting this analysis significantly, for completeness we also consider nuclear shadowing and meson exchange corrections in the deuteron at small values of x.

A. Standard nuclear corrections

The conventional approach to describing nuclear structure functions in the intermediate- and large-x regions is the nuclear impulse approximation, in which the virtual photon scatters incoherently from the individual nucleons bound in the nucleus [11, 12]. Early attempts [13–17] to compute the nuclear corrections in deuterium, as well as some more recent experimental analyses [18–23], utilized simple *ansätze* to account for the nuclear smearing, some of which were rather *ad hoc* or suffered from various shortcomings (for reviews see *e.g.* Refs. [24, 25]). More recent efforts have focussed on deriving relations between the deuteron and free nucleon structure functions more rigorously within well-defined theoretical frameworks.

Within a covariant framework the nuclear structure function can be written as a product of the virtual photon – bound nucleon and nucleon–deuteron scattering amplitudes [12, 26], which, for x not too close to 1, can be systematically expanded in powers of the bound nucleon momentum relative to the nucleon mass, $\boldsymbol{p}/M$. Keeping terms up to order $\boldsymbol{p}^2/M^2$, the nuclear structure function can be written as a convolution of the bound nucleon structure function and the distribution of nucleons in the nucleus [8].

Because the struck nucleon is off its mass shell with virtuality $p^2 = p_0^2 - \boldsymbol{p}^2 < M^2$, its structure function can in principle depend on p^2, in addition to x and Q^2. However, since the deuteron binding energy is only $\approx 0.1\%$ of its mass and the typical nucleon momentum in the deuteron is $|\boldsymbol{p}| \sim 130$ MeV, the *average* nucleon virtuality $\sqrt{p^2}$ will only be $\sim 2\%$ smaller than the free nucleon mass. One can therefore approximate the bound nucleon structure function for x not too close to 1 by its on-shell value, in which case the deuteron structure function can be written as a convolution of the free nucleon (proton p or neutron n) structure function and a momentum distribution $f_{N/d}$ of nucleons in the deuteron,

$$F_2^d(x, Q^2) \approx F_2^{d\,(\mathrm{conv})}(x, Q^2) = \sum_{N=p,n} \int_{y_{\min}}^{y_{\max}} dy\, f_{N/d}(y, \gamma)\, F_2^N\left(\frac{x}{y}, Q^2\right). \qquad (1)$$

The distribution $f_{N/d}$ (also called the "smearing function") is in general a function of the

4

deuteron's momentum fraction carried by the struck nucleon, $y = (M_d/M)(p \cdot q/p_d \cdot q)$, where q is the virtual photon momentum, and p_d and M_d are the deuteron four-momentum and mass. At finite Q^2, however, it also depends on the variable $\gamma = \sqrt{1 + 4x^2 M^2/Q^2}$, which in the deuteron rest frame can be thought of as the virtual photon "velocity", $\gamma = |\boldsymbol{q}|/q_0$. In the Bjorken limit the function $f_{N/d}$ becomes independent of γ, but for moderate Q^2 the dependence on γ becomes important at $x \gtrsim 0.85$ [10].

The smearing function $f_{N/d}$ is computed from the deuteron wave function $\Psi_d(\boldsymbol{p})$, and accounts for the effects of Fermi motion and binding energy of the nucleons in the nucleus, as well as kinematic $1/Q^2$ corrections; in the WBA the combined effects of these are given by [9, 10, 27]

$$f_{N/d}^{\text{(WBA)}}(y, \gamma) = \int \frac{d^3\boldsymbol{p}}{(2\pi)^3} \left(1 + \frac{\gamma p_z}{M}\right) \mathcal{C}(y, \gamma) \, |\Psi_d(\boldsymbol{p})|^2 \, \delta\left(y - 1 - \frac{\varepsilon + \gamma p_z}{M}\right), \qquad (2)$$

where p_z is the longitudinal component of $\boldsymbol{p}$, and the separation energy $\varepsilon \equiv p_0 - M = M_d - E_p - M \approx \varepsilon_d - \boldsymbol{p}^2/2M$ by expanding the recoil nucleon energy $E_p = \sqrt{M^2 + \boldsymbol{p}^2}$ for small $\boldsymbol{p}$. The finite-Q^2 correction factor is [9, 10]

$$\mathcal{C}(y, \gamma) = \frac{1}{\gamma^2} \left[1 + \frac{(\gamma^2 - 1)}{y^2} \left(1 + \frac{2\varepsilon}{M} + \frac{3p_\perp^2 - 2\boldsymbol{p}^2}{2M^2}\right)\right], \qquad (3)$$

where $p_\perp$ is the transverse nucleon momentum, and becomes unity in the Bjorken limit, $\mathcal{C}(y, \gamma \to 1) \to 1$. The resulting distribution function is sharply peaked around $y \approx 1$, with the width determined by the amount of binding (in the limit of zero binding, i.e., for a free proton or neutron, it would be a δ-function at $y = 1$). At finite Q^2 (or $\gamma \neq 1$) the function becomes somewhat broader, effectively giving rise to more smearing for larger x or smaller Q^2. For nonrelativistic kinematics the variable y is bounded by $y_{\min} = x(1 - 2\varepsilon_d M/Q^2)$ and $y_{\max} = 1 + \gamma^2/2 + \varepsilon_d/M$, so that its maximum allowed value, even in the Bjorken limit, is approximately 1.5 instead of $M_d/M \approx 2$.

The deuteron wave function $\Psi_d(\boldsymbol{p})$ contains the usual nonrelativistic S- and D-states, and is normalized according to $\int d^3\boldsymbol{p} \, |\Psi_d(\boldsymbol{p})|^2 /(2\pi)^3 = 1$. In the numerical calculations we use several nonrelativistic deuteron wave functions, the high-precision AV18 [28] and CD-Bonn [29] NN potentials, as well as the older Paris potential [30] for comparison with earlier work. As illustrated in Fig. 1, where we show the computed ratio $R^{d/N}$ relative to that for the AV18 wave function, the differences between these are very small for $x \lesssim 0.7$. At larger x the differences become more visible, reflecting the greater role played by the large-y tail of the
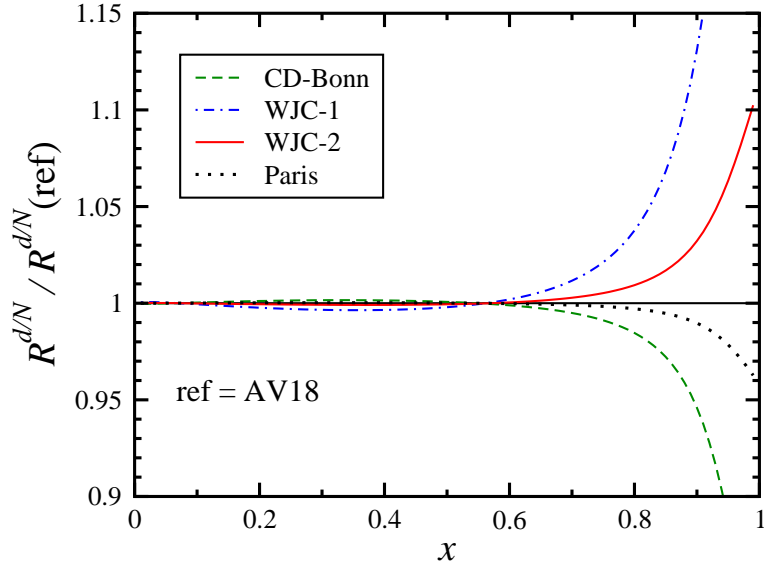
FIG. 1: Dependence of the ratio $R^{N/d} = F_2^d/F_2^N$ on the deuteron wave function, for the nonrelativistic CD-Bonn [29] (dashed) and Paris [30] (dotted) models, as well as the relativistic WJC-1 (dot-dashed) and WJC-2 [31] (solid) models, relative to the ratio for the AV18 wave function [28].

smearing function, with the CD-Bonn wave function giving an approximately 10% smaller ratio for $x \sim 0.9$. The result with the older Paris wave function agrees with the AV18 to within 1% over this x range. The large-y tail in turn reflects greater sensitivity to the short-distance parts of the NN interaction, where the validity of the nonrelativistic approximation itself is more questionable. For comparison we also show the ratios in Fig. 1 computed with the relativistic WJC-1 and WJC-2 wave functions [31] (see Sec. II B below). Because the relativistic wave functions contain higher orders in $\boldsymbol{p}/M$, they exhibit larger high-momentum tails, which leads to larger $R^{d/N}$ ratios than for nonrelativistic wave functions. Generally, the wave functions with the largest D-state probabilities (7.4% for WJC-1 $cf.$ 4.8% for CD-Bonn) give rise to the largest distributions at large y, and hence the highest $R^{d/N}$ ratios at large x.

B.   Relativistic effects

Since quarks at large momentum fractions x are most likely to originate in nucleons carrying a large momentum fraction y themselves, the effects of relativity will be increasingly more important as $x \to 1$. A relativistic framework is therefore required to describe DIS from

the deuteron at large x. The effects of relativistic kinematics are generally straightforward to implement, while the dynamical effects of relativity require model dependent assumptions.

A framework which incorporates the kinematic effects of relativity was proposed recently [27] using collinear factorization applied to nuclear DIS. Assuming factorization of the (scalar) nucleon hadronic tensor and the single-nucleon four-momentum distribution, a smearing function (labeled "AQV") could be obtained which properly takes into account relativistic kinematics [27],

$$f_{N/d}^{(\mathrm{AQV})}(y,\gamma) = \int \frac{d^3\boldsymbol{p}}{(2\pi)^3} \frac{y}{\gamma^2} \left[1 + \frac{(\gamma^2 - 1)}{y^2} \frac{(3p_\perp^2 + 2p^2)}{2M^2} \right] |\Psi_d(\boldsymbol{p})|^2 \, \delta \left(y - \frac{p_0 + p_z}{M} \right). \quad (4)$$

One can easily show that the function $f_{N/d}^{(\mathrm{AQV})}$ reduces to the WBA expression (2) in the nonrelativistic limit, *i.e.*, at order $\boldsymbol{p}^2/M^2$. Note that for relativistic kinematics the maximum value for y is determined from $y_{\max} = M_d/M + x(M^2 - p^2)/Q^2$; since the nucleon virtuality p^2 is unbounded from below, at any finite Q^2 the fractional momentum y is effectively unbounded from above. In practice, though, taking $y_{\max} \approx M_d/M$, as would be the case in the Bjorken limit, provides a relatively good approximation to the exact integral for values of $x \lesssim 1$.

The effects of relativistic kinematics on the WBA smearing function are illustrated in Fig. 2, where the ratio $R^{d/N}$ for the smearing function with nonrelativistic kinematics (2) is plotted relative to the same ratio using the relativistic expression (4). To isolate the kinematic effects on $R^{d/N}$, the same AV18 wave function is used in both cases. The relativistic effects are negligible for $x \lesssim 0.6$, but grow to around 5% at $x \approx 0.9$, before increasing rapidly as $x \to 1$.

Taking the full spin and Lorentz structure of the off-shell nucleon hadronic tensor into account, a formalism for DIS from bound nucleons which incorporates both relativistic kinematics and dynamics was developed in Ref. [26]. This analysis identified the conditions under which the nuclear structure function could be expressed in the factorized convolution form (1), but found that in general these are not satisfied relativistically. A follow-up study [32] (referred to as "MST") showed, however, that one could isolate a "relativistic convolution" component from the total F_2^d, together with additive corrections associated with the relativistic P-state components of the deuteron wave function and nucleon off-shell corrections. Although the relativistic convolution component of F_2^d is not unique (only the total structure function is), a natural choice which respects baryon number conservation in
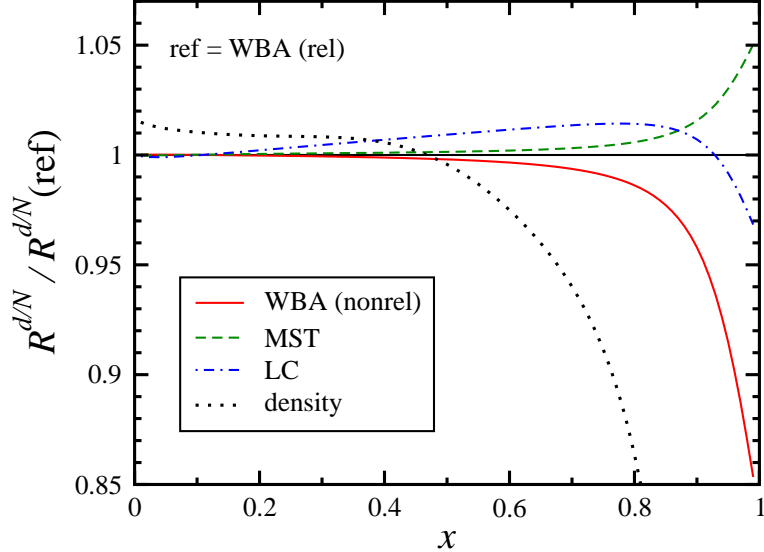
FIG. 2: Dependence of the ratio $R^{N/d} = F_2^d/F_2^N$ on the nuclear model and effects of relativity, relative to the ratio with the WBA model with the AV18 wave function and relativistic kinematics for $\gamma = 1$. The nonrelativistic WBA model [9, 10] (solid), the MST relativistic convolution [32] (dashed), and the light-cone model [33] (dot-dashed) illustrate the nuclear model dependence, with the nuclear density extrapolation model [34] (dotted) shown for reference.

the deuteron (in the $\gamma \to 1$ limit) is [32]

$$f_{N/d}^{(\mathrm{MST})}(y) \;=\; \frac{M_d^2}{4M} \int \frac{d^3\boldsymbol{p}}{(2\pi)^3} \frac{y}{p_0} \, |\Psi_d(\boldsymbol{p})|^2 \, \theta(p_0) \, \delta\left(y - \frac{p_0 + p_z}{M}\right). \tag{5}$$

Expanding the integrand in Eq. (5) to order $\boldsymbol{p}^2/M^2$ one can again show explicitly that $f_{N/d}^{(\mathrm{MST})}$ reduces to the nonrelativistic WBA smearing function in Eq. (2) in the $\gamma \to 1$ limit.

In Eq. (5) the relativistic deuteron wave function $\Psi_d(\boldsymbol{p})$ formally contains, in addition to the S- and D-state components, also the singlet and triplet P-state contributions associated with negative nucleon energies. To compute the relativistic smearing function we use the relativistic deuteron wave functions from Ref. [31] with the WJC-1 model, which has an admixture of pseudoscalar and pseudovector πNN couplings, and the WJC-2 model, which has only the pseudovector coupling. The WJC-1 model generally has larger high-momentum components than the WJC-2 model, as evidenced in its larger D-state probability, and the pseudoscalar πNN coupling leads to significantly larger P-state wave functions than for the pure pseudovector model. The harder WJC-1 wave function gives rise to a ratio $R^{d/N}$ which at $x \gtrsim 0.6$ is larger than that for WJC-2, and as observed in Fig. 1 the larger high-

8

momentum tails in both the relativistic wave functions yield larger contributions to F_2^d (and $R^{d/N}$) at large x than in the nonrelativistic models.

To assess the model dependence associated with the choice of smearing function, in Fig. 2 we show the ratio $R^{d/N}$ computed from the MST smearing function (5) relative to the WBA model with relativistic kinematics (4). The differences are $< 1\%$ for $x < 0.8$, rising to $\sim 5\%$ as $x \to 1$. For comparison we also show the ratio computed using an early light-cone prescription for nuclear DIS [33], which has been previously used in some F_2^d data analyses [35]. In this approach the bound nucleons are taken to be on their mass shells, with the struck nucleon energy $p_0 = E_p$, but with energy not conserved at vertices. The light-cone smearing function (for $\gamma = 1$) is given by [33]

$$f_{N/d}^{(\mathrm{LC})}(y) \; = \; \int \frac{d^3\boldsymbol{p}}{(2\pi)^3} \left| \Psi_d^{(\mathrm{LC})}(\boldsymbol{p}) \right|^2 \delta\left(y - 1 - \frac{p_z}{E_p} \right), \tag{6}$$

which preserves baryon number and implies that the entire momentum of the deuteron is carried by the nucleons. Note that for consistency the light-cone wave function $\Psi_d^{(\mathrm{LC})}(\boldsymbol{p})$ in Eq. (6) should be computed using light-front dynamics (or in the infinite momentum frame), although in practice ordinary rest-frame wave functions are used. Because the light-cone prescription does not explicitly incorporate nuclear mesons, which are responsible for nuclear binding, it effectively corrects the deuteron structure function for the effects of Fermi motion only. This is reflected in the ratio $R^{d/N}$ in Fig. 2 being larger at intermediate x ($0.2 \lesssim x \lesssim 0.8$) than in the models which do account for nuclear binding. Nevertheless, the differences between $R^{d/N}$ computed with the light-cone smearing function $f_{N/d}^{(\mathrm{LC})}$ and the others in Fig. 2 are less than 2–3% for all x. In practice, because of the inconsistency of mixing rest-frame wave functions with the light-cone smearing function (6), as well as the need for finite-Q^2 corrections in the smearing function (which are not available for the light-cone or MST models), we shall restrict our analysis to the WBA and AQV smearing functions.

Finally, we compare the microscopic calculations with a qualitative model in which the ratio $R^{d/N}$ is extrapolated from data on the ratio of heavy nuclei to deuterium structure functions assuming scaling with nuclear density [36]. Using the empirical nuclear density for ^{56}Fe and an *ansatz* for the charge density of deuterium [34, 37], the ratio is obtained from $R^{d/N} \approx 1 + (R^{\mathrm{Fe}/d} - 1)/4$ [34], which implies similar x dependence of the nuclear corrections in ^{56}Fe and deuterium. Consequently, $R^{d/N}$ in the density model has a significantly larger

depletion at $x \sim 0.6$ and a rise above unity which does not set in until $x \sim 0.8$. This is significantly higher than typically found in smearing models, as reflected in the rapidly falling ratio $R^{d/N}$ in Fig. 2 for the density model compared with the other calculations [38]. The nuclear density scaling is also in disagreement with recent data on light nuclei [39] which do not support simple A-dependent or density-dependent fits to the nuclear structure function ratios. Because of this, as well as the difficulties in defining physically meaningful nuclear densities for deuterium [37], we do not consider the density model sufficiently quantitative, especially at large x, to be reliably employed in global PDF analyses.

C. Off-shell corrections

The discussion of nuclear effects above has been under the assumption that the structure function of the bound nucleon in the convolution formula (1) does not change inside the nucleus, and can be approximated by the on-shell F_2^N. With the inclusion of off-shell and relativistic corrections, it was shown in Ref. [32] that the convolution formula receives nonfactorizable corrections associated with higher powers of the bound nucleon momentum $\boldsymbol{p}/M$ and contributions proportional to $p^2 - M^2$, $F_2^d = F_2^{d\,(\text{conv})} + \delta^{(\text{off})} F_2^d$. The correction $\delta^{(\text{off})} F_2^d$ was estimated within a simple quark–spectator model [32], with the parameters of the quark–nucleon correlation functions fitted to proton and deuteron F_2 data. The overall effect is a reduction of about 2% of F_2^d compared to the on-shell (convolution) approximation, as illustrated in Fig. 3. A simple parametrization of $\delta^{(\text{off})} F_2^d$ relative to the total F_2^d in the model of Ref. [32] was given in Ref. [1].

Within the nonrelativistic WBA model (or the relativistic AQV model) inclusion of explicit off-shell dependence in the bound nucleon structure function leads to a generalization of Eq. (1) in which F_2^d is expressed as a two-dimensional convolution in terms of y and the nucleon virtuality p^2 [8, 27]. For small values of $|p^2 - M^2|/M^2 \ll 1$, one can expand the off-shell structure function in a Taylor series about $p^2 = M^2$ [9],

$$F_2^N(x, Q^2, p^2) \;=\; F_2^N(x, Q^2) \left(1 + \delta f_2(x, Q^2) \frac{p^2 - M^2}{M^2} \right), \qquad (7)$$

where the coefficient of the $p^2 - M^2$ term is given by the p^2 derivative of the structure function,

$$\delta f_2(x, Q^2) \;=\; \left. \frac{\partial \log F_2^N(x, Q^2, p^2)}{\partial \log p^2} \right|_{p^2 = M^2}. \qquad (8)$$
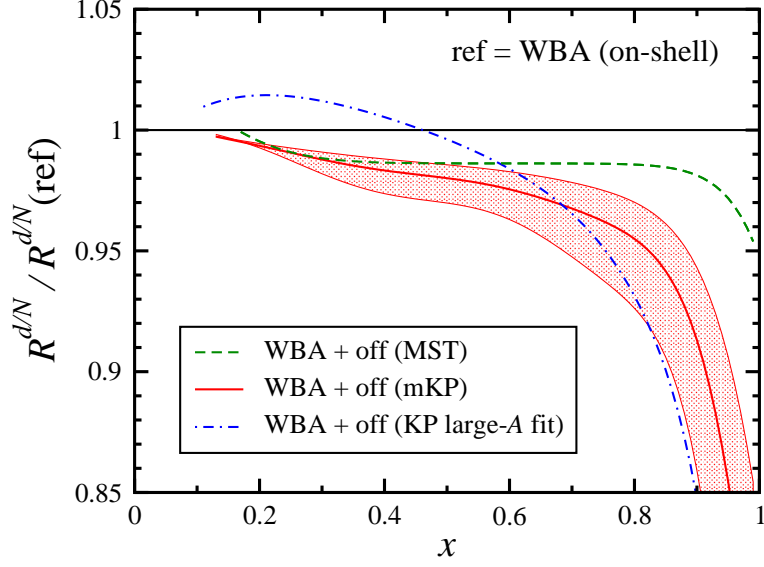
10

FIG. 3: Dependence of the ratio $R^{N/d} = F_2^d/F_2^N$ on the off-shell corrections to the nucleon structure function, relative to the on-shell WBA model. The range of off-shell behaviors includes the MST off-shell model [32] (dashed), the Kulagin-Petti model [9] modified for the case of deuterium (mKP, solid and shaded band), and the Kulagin-Petti phenomenological fit to large-A structure function data [9] (dot-dashed).

Assuming that δf_2 is independent of the nucleus A, a phenomenological fit to all available nuclear F_2^A/F_2^d data, with A ranging from ^{4}He to ^{207}Pb, found for the nonrelativistic model [9]

$$\delta f_2^{(\text{fit})} = C_N(x - 0.05)(x - x_0)(1 + x_0 - x), \qquad (9)$$

with the best-fit parameters $C_N = 8.1(3)$ and $x_0 = 0.448(5)$. The zero crossings of δf_2^{fit} at $x = 0.05$ and $x = x_0$ give rise to an enhanced $R^{d/N}$ ratio for $x \lesssim 0.45$, and a sharp drop for $x \gtrsim 0.6$ compared with the on-shell result, as Fig. 3 illustrates. This reflects the general features of the data on the nuclear EMC ratios $R^{A/d} \equiv F_2^A/F_2^d$, which the fitted off-shell correction δf_2^{fit} mimics [9]. Since one assumes the same shape for the off-shell correction in the deuteron as in heavy nuclei, the x dependence of $R^{d/N}$ in this model is similar to that of $R^{A/d}$. This feature is reminiscent of the nuclear density model [34] (see Sec. II B) which scales the magnitude of $R^{A/d}$ to the deuteron, but assumes the same x dependence. While this scaling may be reasonable for large-A nuclei, we do not believe that an extrapolation all the way to the deuteron is likely to be reliable, especially at large x. In addition, the

11

phenomenological fit (9) does not conserve the total baryon number in the nucleus. Some cancellation is found between the off-shell and nuclear shadowing corrections [9]. However, since shadowing contains important higher twist in addition to leading twist contributions, the cancellation cannot be exact at all Q^2.

To avoid these problems we choose instead to use a microscopic model proposed by Kulagin & Petti [9] (see also Ref. [8]), but modified to apply to the specific case of the deuteron in the valence quark region at large x. Here the valence quark distribution can be expressed through a spectral representation as

$$q_v(x, p^2) = \int ds \int_{-\infty}^{k^2_{\max}} dk^2 \, D_{q/N}(s, k^2, x, p^2), \tag{10}$$

where k^2 is the virtuality of the quark, with maximum value $k^2_{\max} = x(p^2 - s/(1-x))$, and $s = (p - k)^2$ is the mass of the spectator quark system. The spectral function $D_{q/N}$ can be approximated by a factorized form

$$D_{q/N} \approx \delta(s - s_0) \, \Phi(k^2, \Lambda(p^2)), \tag{11}$$

where the function Φ describes the distribution of valence quarks with virtuality k^2 in an off-shell nucleon with invariant mass p^2, and for simplicity the spectator quark spectrum is assumed to be given by a single mass s_0. The nucleon off-shell dependence is parametrized through the p^2 dependence of the large-k^2 cut-off mass parameter $\Lambda(p^2)$ in Φ. From a fit to the free proton data one finds the value $s_0 = 2.1$ GeV^2 [9]. The scale Λ can be related to the nucleon confinement radius, $\Lambda \sim 1/R_N$, so that the dependence of Λ on p^2 reflects a change in the size of the bound nucleon in a nuclear medium. The off-shell function δf_2 can then be written as [9]

$$\delta f_2 = c + \frac{\partial \log q_v}{\partial x} h(x), \tag{12}$$

where

$$h(x) = x(1-x)\frac{(1-\lambda)(1-x)M^2 + \lambda s_0}{(1-x)^2 M^2 - s_0} \tag{13}$$

and

$$\lambda = \partial \log \Lambda^2 / \partial \log p^2 \big|_{p^2 = M^2} . \tag{14}$$

12

In terms of the confinement radius R_N the parameter λ can also be written as $\lambda = -2(\delta R_N/R_N)(\delta p^2/M^2)$, where $\delta p^2 = \int dy\,(p^2 - M^2)f_{N/d}(y)$ is the average nucleon virtuality in the deuteron.

In the analysis of Ref. [9], λ and c were chosen to reproduce the shape of the KP fit (9), finding $\lambda = 1.03$ — a value that corresponds to an increase in the confinement radius of $\delta R_N/R_N \sim 9\%$, as may be expected for a heavy nucleus such as ^{56}Fe. Here we modify the model to the specific case of the deuteron, for which $\delta R_N/R_N \approx 1.5 - 1.8\%$ [40]. For δp^2 we take a range of smearing functions computed with different wave functions (AV18, CD-Bonn, WJC-1, WJC-2), as well as relativistic versus nonrelativistic kinematics, resulting in the range $\delta p^2/M^2 \approx -3.6\%$ to -6.5%. This gives λ in the range $0.46 - 1.00$, with a central value of 0.65. Finally, the normalization coefficient c is computed by requiring that the off-shell corrections do not modify the valence quark number,

$$\int_0^1 dx\, q_v(x)\, \delta f_2(x) \;=\; 0, \tag{15}$$

which leads to the constraint

$$c \;=\; \int_0^1 dx\, \frac{\partial q_v(x)}{\partial x}\, h(x). \tag{16}$$

The resulting ratio $R^{d/N}$ with the off-shell corrections in this "modified Kulagin-Petti" (mKP) model is indicated in Fig. 3 by the shaded band, which reflects the uncertainty in the parameter λ. For $x \lesssim 0.5$, the ratio with the mKP off-shell correction is similar to that with the MST off-shell model, ranging between 1% and 3%, but grows with increasing x. At $x = 0.9$ the off-shell ratio is some $5\% - 15\%$ smaller than the on-shell ratio. These uncertainties will propagate through the global analysis and affect the precision to which PDFs at large x can be determined, as discussed in Sec. IV. Note that in principle the fits should be performed using the same deuteron wave function to compute both the smearing function and the off-shell correction (namely, for a specific value of $\delta p^2/M^2$ rather than the above range). However, given the uncertainty in $\delta R_N/R_N$, as well as the assumptions inherent in the off-shell model itself, we take the conservative approach of including the total off-shell uncertainty in the fits for each smearing function.

D. Nuclear shadowing

At intermediate and large values of x the nuclear impulse approximation, embodied in the convolution approximation of Eq. (1), provides a reasonable basis for computing nuclear structure functions. At small values of x, however, this approximation becomes less reliable and the probability of scattering from more than one nucleon in the nucleus becomes relevant. For the case of the deuteron one can compute the shadowing correction arising from the double scattering of the virtual photon from both nucleons using the Glauber expansion in the eikonal approximation (for a review see Ref. [41]).

In the target rest frame one can view nuclear DIS at small x in terms of virtual photon fluctuations into $q\bar{q}$ pairs of mass $m_{q\bar{q}}$, which then interact with the target. The propagation length of the virtual $q\bar{q}$ state is $\Delta l \sim 2\nu/(Q^2 + m_{q\bar{q}}^2)$ with ν the virtual photon energy. If this exceeds the inter-nucleon separation (~ 2 fm), then the hadronic state can interact with different nucleons as it passes through the nucleus. For large $\nu \gg m_{q\bar{q}}$ the propagation length becomes $\Delta l \sim 1/Mx \gtrsim 2$ fm, so that shadowing should start to appear at $x \lesssim 0.1$.

At low Q^2 the spectrum of $q\bar{q}$ states can be well approximated by vector mesons (ρ^0, ω, ϕ), while at high Q^2 the interaction is most efficiently described through diffractive scattering of the $q\bar{q}$ pair from partons, parametrized by Pomeron exchange. Such a two-phase model was adopted in Refs. [42–45] to compute the shadowing corrections in deuterium and heavy nuclei. The vector meson dominance contribution vanishes at sufficiently high Q^2, but in the $Q^2 \sim$ few GeV^2 range it is in fact responsible for the majority of the Q^2 variation [43].

An additional double scattering contribution arises from the interaction of the virtual photon with a mesons ($\pi, \rho, \ldots$) exchanged between the nucleons in the deuteron [43, 46]. This correction is mostly positive at small x ("antishadowing"), and partly cancels some of the shadowing arising from Pomeron exchange and vector meson dominance [43].

In our analysis we parametrize the total deuterium shadowing correction from Ref. [43] (similar values were obtained in Refs. [42, 45, 47]) as an additive contribution to the deuteron structure function, $F_2^d \rightarrow F_2^d + \delta^{(\mathrm{shad})} F_2^d$. The resulting correction ranges from about 1.5% at $x = 10^{-2}$ to about 3% for $x \leq 10^{-5}$. The effect of such corrections on PDFs in the region of interest of the current analysis is negligible.

III. DATA SELECTION AND FITTING PROCEDURES

The data sets used in this analysis are the same ones chosen in the recent CTEQ6X analysis [1]. Since this represents an extension of the previous work, utilizing the same data sets facilitates an easy comparison with the results presented there. The data sets include charged lepton DIS on proton and deuteron targets, lepton pair production with a proton beam on proton and deuteron targets, W-lepton asymmetry and W asymmetry data sets from $\overline{p}p$ interactions, and $\gamma + $ jet and inclusive jet data sets from the Tevatron. As in Ref. [1], we adopt for our main fits the cuts $Q^2 > 1.69$ GeV^2 and $W^2 > 3$ GeV^2. Before proceeding with the discussion of the fits, it is useful to briefly review the flavor differentiation at large x provided by the various types of data.

In the large-x region the relevant quark PDFs are those for the u and d quarks. Consider first *charged lepton DIS*. For large values of x the structure functions are given, to lowest order in α_s, by

$$F_2^p(x, Q^2) \approx \frac{x}{9} \left(4u(x, Q^2) + d(x, Q^2) \right) \tag{17}$$

and

$$F_2^N(x, Q^2) \approx \frac{5x}{18} \left(u(x, Q^2) + d(x, Q^2) \right), \tag{18}$$

where the superscript N denotes the structure function of an isoscalar nucleon target obtained from deuterium data by including nuclear corrections. If one had sufficient data of both types, then the separate u and d PDFs could be disentangled. The problem, however, is that variations in the nuclear corrections cause variations in the extracted F_2^N which, in turn, causes variations in the extracted d PDF. The u PDF is relatively better determined since, at large values of x, the d/u ratio is small and the u PDF enters with a weight which is four times larger than that for the d PDF in F_2^p. Thus, the nuclear corrections primarily affect the d PDF.

Next, consider *lepton pair production*. Since the PDFs enter in a manner different than for charged lepton DIS, one may hope to use these data to constrain the d PDF. Using lowest order kinematics one has

$$M_{ll}^2 = x_1 x_2\, s \quad \text{and} \quad x_F = x_1 - x_2, \tag{19}$$

where M_{ll} is the lepton pair invariant mass, $x_F = 2p_z/\sqrt{s}$ is the scaled longitudinal momentum of the pair, and x_1 and x_2 denote the beam and target momentum fractions, respec-

tively. The region of interest for typical fixed target experiments is large x_1 and small x_2, where the proton-proton cross section is (neglecting the Q^2 dependence)

$$\sigma_{DY}(pp) \ \propto \ \overline{u}(x_2) \left(4u(x_1) + d(x_1) \frac{\overline{d}(x_2)}{\overline{u}(x_2)} \right). \tag{20}$$

At small values of $x_2 \ll 1$ one has $\overline{u}(x_2) \approx \overline{d}(x_2)$ so that this cross section is approximately given by the same linear combination of PDFs as enters F_2^p, namely, $4u(x_1) + d(x_1)$. This situation is not helped significantly even if one considers lepton pair production on a deuteron target since for small x_2 the nuclear effects discussed previously are small and, using isospin invariance, the proton-neutron cross section is

$$\sigma_{DY}(pn) \ \propto \ \overline{d}(x_2) \left(4u(x_1) + d(x_1) \frac{\overline{u}(x_2)}{\overline{d}(x_2)} \right). \tag{21}$$

Thus, one is still sensitive to the same linear combination of PDFs at large values of x_1, as probed by available data.

Next let us examine data for *jet production*. The cross section for this process involves combinations of quark–quark, quark–gluon, and gluon–gluon scattering subprocesses. The large-x gluon PDF is constrained mostly by just such data, assuming that the quark PDFs are fixed. Therefore, if the d PDF is varied it is possible for the gluon PDF to compensate the change in the jet cross section by a similar but opposite variation in its magnitude. As a consequence, we can also expect the gluon PDF to be sensitive to nuclear corrections, and anti-correlated to the d-quark PDF.

This leaves the data for the W *asymmetry*, A_W, and W-*lepton asymmetry*, A_l. These asymmetries are sensitive to the d/u ratio; however, the data coverage extends at most to W rapidities of $y_W \approx 2.6$, which corresponds to $x \approx 0.6$. The data for A_l extend to lepton rapidities of $y_e \approx 3$. This formally corresponds to $x \approx 0.8$, were it not for the smearing induced by the lepton decay vertex, which reduces this to $x \approx 0.6$ (see Sec. IV D).

Thus, one can see that to constrain the d PDF in the large-x region using existing data one must use DIS data on deuterium, and there one is faced with the necessity of addressing the issue of nuclear corrections. In Sec. V below, methods of reducing this dependence on the nuclear corrections will be discussed.

IV. FIT RESULTS

The global fits discussed here were performed using the same fitting package and techniques as described in Ref. [1]. We refer to these as the "CJ" (CTEQ-Jefferson Lab) PDF fits. The nuclear effects in the deuteron were computed using the smearing function (4) with relativistic kinematics. To quantify the systematic uncertainty on the PDFs due to the nuclear corrections, we used the AV18, CD-Bonn, WJC-1 and WJC-2 deuteron wave functions, with on-shell nucleons or off-shell corrections from the range allowed in the mKP model, as discussed in Sec. II. We also considered a generalization of the d-quark parametrization at the initial scale $Q_0^2 = 1.69$ GeV^2 that allows the d/u ratio to have an arbitrary value in the $x \to 1$ limit, as opposed to either 0 or infinity as with standard parametrizations used in global fits.

A. Impact of nuclear corrections

To understand the impact of the nuclear smearing and off-shell corrections, it is useful to examine the ratio of F_2 on a deuterium target to that on an idealized isoscalar target $N = p + n$. To simplify the comparison we take a "toy model" for the input nucleon structure function, $F_2^N \sim (1-x)^3$, and compute the deuteron structure function from the convolution approximation in Eq. (1) with the smearing function calculated using the AV18 deuteron wave function. The resulting ratio $R^{d/N}$ is illustrated in Fig. 4 (dashed curve), and compared with the ratio computed including nucleon off-shell corrections from the mKP model (solid and shaded band), and, for reference, also with the nuclear density extrapolation model (dotted). As anticipated from Fig. 3, the effect of the off-shell corrections is a further suppression of $R^{d/N}$ over most of the range of x, with the ratio now rising above unity for $x \gtrsim 0.7$. The dip in the $R^{d/N}$ ratio in the density model is more pronounced than in the smearing models, even compared with the largest off-shell corrections, and has a shape that essentially follows that of ratios of structure functions of heavy nuclei, such as ^{56}Fe, to deuterium.

Qualitatively, implementing the nuclear corrections is equivalent to dividing the deuterium data by $R^{d/N}$, thereby yielding results for an isoscalar target. In actuality, the corrections involve convolutions as well as realistic F_2^N inputs instead of the simple $\sim (1-x)^3$
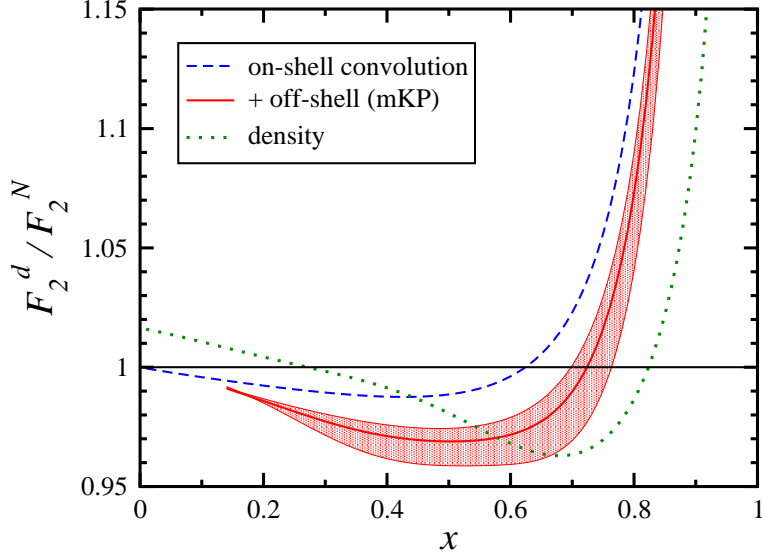
FIG. 4: Deuterium to isoscalar nucleon ratio $R^{d/N} = F_2^d/F_2^N$ using the convolution approximation in Eq. (1) for a "toy model" input $F_2^N \sim (1-x)^3$, without off-shell corrections (dashed) and with the mKP off-shell corrections (12) included (solid and shaded band). For comparison the ratio with the nuclear density extrapolation model (dotted) is also shown.

form we use for illustration. However, the impact of the nuclear corrections on fits of the d-quark distribution can be understood from the following simple argument, which does not depend on these details. When F_2^d/F_2^N is less than one, the removal of the nuclear effects increases the data and therefore yields a larger d PDF than one would have had if the nuclear effects were ignored. Conversely, if the ratio is greater than one, the fitted d PDF will be reduced relative to that extracted from uncorrected data. From the ratio in Fig. 4 one can see that there will be an increase in the d PDF for $x \lesssim 0.6 - 0.7$ (depending on the size of the off-shell corrections), while the Fermi smearing rise in the ratio leads to a decrease in the fitted d PDF for $x \gtrsim 0.6 - 0.7$.

B. d/u ratio

Since the d-quark PDF is most affected by variations in the nuclear corrections, with the u quark relatively unchanged, the results of the fits are best summarized by examining the ratio of d to u PDFs. This ratio is also of theoretical interest as its limiting value as $x \to 1$ is a sensitive indicator of nonperturbative quark-gluon dynamics in the nucleon [48, 49]. The
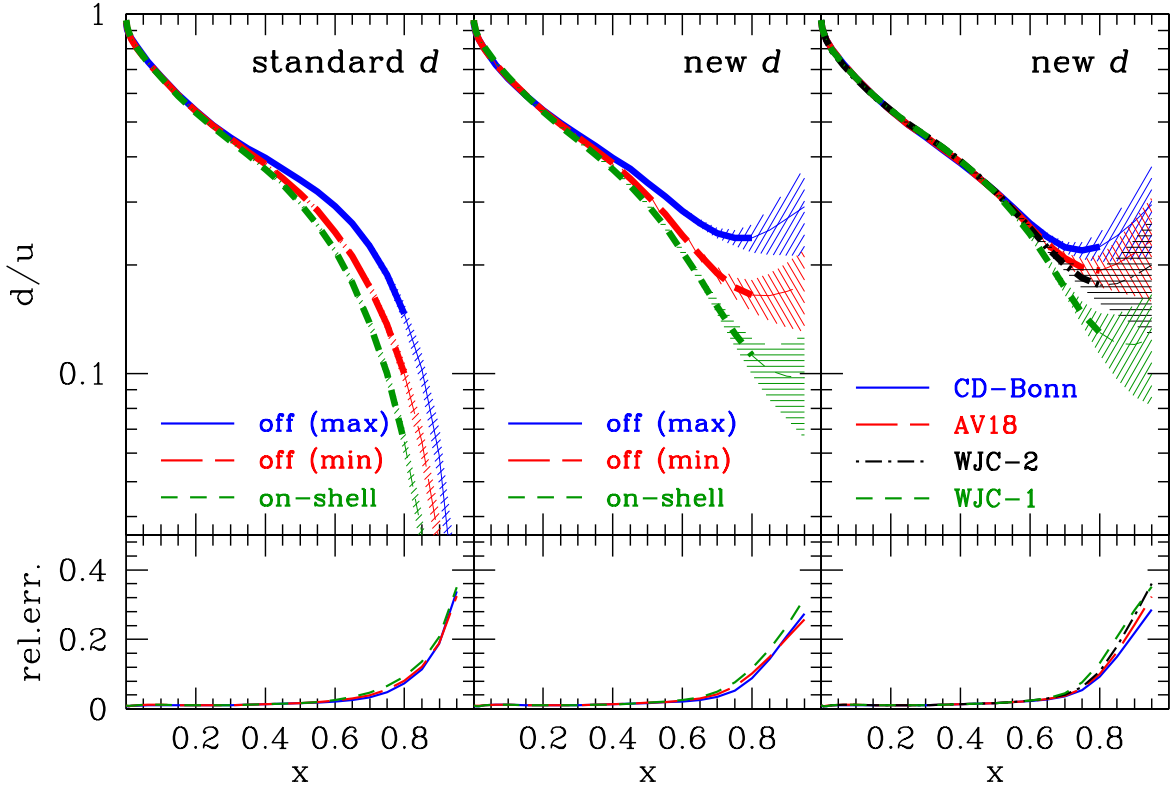
FIG. 5: The d/u ratio at $Q^2 = 10$ GeV^2 obtained with different choices of d-quark parametrization and nuclear corrections: (*left panel*) standard d-quark parametrization [1] and AV18 deuteron wave function for several off-shell corrections models; (*middle panel*) modified d-quark parametrization (22) for the same nuclear corrections; (*right panel*) dependence on the deuteron wave function for a fixed off-shell correction (mKP). The shaded bands and bottom panels show the $\Delta\chi = 1$ PDF errors and the relative PDF errors on the d/u ratio, respectively. The thinner lines above $x \approx 0.8$ denote extrapolations into unmeasured regions.

effect of nuclear corrections on the gluon PDFs will be discussed in Sec. IV E.

In Fig. 5 the d/u ratio is shown for various models of nuclear corrections. The left and middle panels show the variation induced by the choice of nucleon off-shell corrections with a fixed (AV18) deuteron wave function. As the magnitude of the off-shell corrections increases, the d/u ratio correspondingly rises. The left panel is obtained using a conventional parametrization for the d PDF which behaves as a power of $(1 - x)$ as $x \to 1$ [1, 2]. The middle panel shows the results of employing a modified form of the d PDF parametrization

at the input scale Q_0^2,

$$d(x, Q_0^2) \longrightarrow d(x, Q_0^2) + a\, x^b\, u(x, Q_0^2), \tag{22}$$

with a and b fitted parameters (see also Refs. [36, 50]). With the conventional parametriza-tions of the d and u PDFs the d/u ratio goes either to zero or infinity as $x \to 1$; with the modified form the ratio $d/u \to a$ as $x \to 1$. The fits, depending on the nuclear correction used, show a slight to marked χ^2 preference for a nonzero value of a, with its value increasing as the off-shell corrections become stronger. The error bands are larger for the case of the modified parametrization since the ratio is not required to go to zero at $x = 1$, so one has a wider range of possibilities for the ratio in the region beyond $x = 0.8$. Note, however, that the relative errors are essentially the same for both parametrizations.

Variations in the choice of the deuteron wave function also affect the extracted d PDF, as shown in the right panel of Fig. 5, where the modified d parametrization (22) is utilized. The resulting spread is comparable in magnitude to that observed for variations in the nucleon off-shell correction models.

Note that the d/u results above $x \approx 0.8$, marked by thinner lines in Fig. 5 for the central values, represent extrapolations of the fitted PDFs and are not constrained directly by data. Correspondingly, the fit errors increase significantly for $x \gtrsim 0.8$, especially for the PDFs using the less restrictive d parametrization (22), as noted above. In all the fits the error bands are calculated using the Hessian technique and correspond to $\Delta\chi = 1$, which was chosen for clarity of the presentation. A larger choice of $\Delta\chi$ would have made it difficult to display the effects of variations in the nuclear models.

Figure 6 shows the total variation in the d/u ratio (cross-hashed band) for all the choices of deuteron wave function and off-shell corrections considered in this analysis, using the modified d-quark parametrization (22). The highest d-quark PDF at large x is obtained with the combination of CD-Bonn wave function and the upper limit of the mKP off-shell correction, while the lowest d quark is obtained with the WJC-1 wave function and no off-shell corrections. The outer band in Fig. 6 (diagonal hashed) shows in addition the uncertainty from the PDF fit. As a reference fit for later use we choose the PDFs extracted using the AV18 and mKP (central) off-shell corrections, which produces a d-quark PDF approximately midway between the upper and lower limits. Above $x \approx 0.8$ the PDFs are not directly constrained by data and represent extrapolations, as indicated by the arrow in
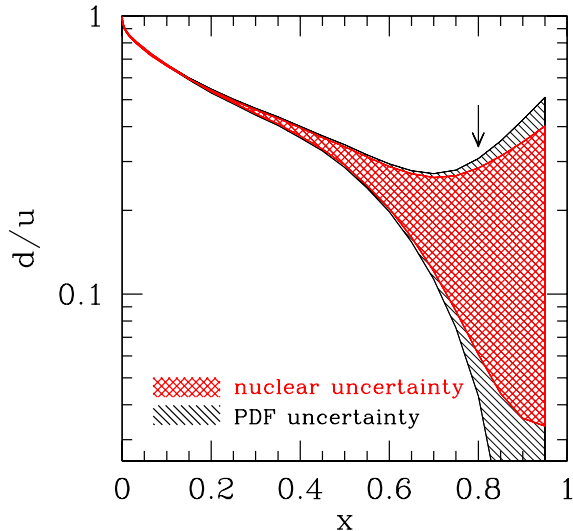
FIG. 6: Full range of variations of the d/u ratio due to deuteron wave function and off-shell corrections (cross-hashed band) and PDF fit uncertainties (diagonal hashed). The arrow indicates the extrapolation region at large x.

Fig. 6.

It is clear that the systematic uncertainty on the extracted d PDF due to the model dependence of the deuteron corrections is considerable. One of the main interests of measuring the d/u ratio at large x is that its limit as $x \to 1$ is sensitive to the nonperturbative structure of the nucleon [48, 49]. However, given the large nuclear model uncertainty, essentially any value of d/u between 0 and ≈ 0.5 is currently allowed, which encompasses most values predicted by the nonperturbative models [48].

The nuclear model uncertainty on the d/u ratio is several times larger than the $\Delta\chi = 1$ PDF uncertainty induced by the experimental errors. Other global fits, such as MSTW08 [3] or CT10 [2], utilize a different criterion to quote the PDF experimental uncertainty, which can be approximately reproduced using $\Delta\chi = 7$. In this case the PDF nuclear uncertainty would be slightly smaller than the experimental uncertainty. Overall, the nuclear and experimental uncertainties are of the same order of magnitude. Progress in constraining the d-quark PDFs at large x will therefore require either a better understanding of nuclear corrections to reduce the nuclear corrections systematics, or the use of a much larger free-nucleon data set sensitive to large-x d quarks than presently available.
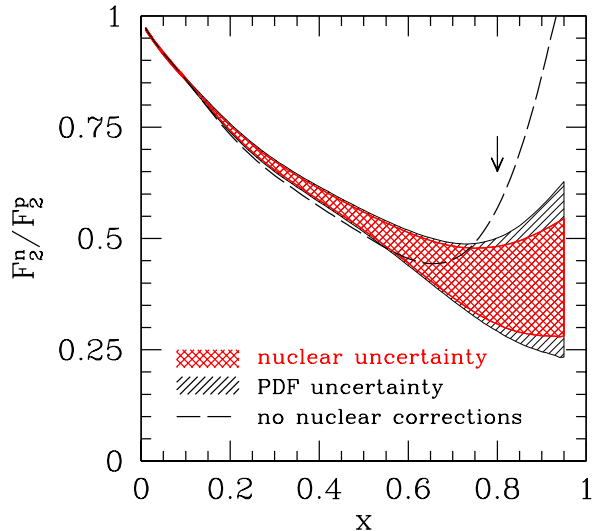
21

FIG. 7: As in Fig. 6, but for the F_2^n/F_2^p ratio. For comparison, the central value of a fit with no nuclear corrections applied is also shown (dashed).

C. Fits of neutron structure functions

The PDFs obtained from our global fit can be used to compute the structure functions of a free neutron, providing an effective method to extract these from inclusive deuteron DIS data, which additionally benefits from information coming from a much wider range of processes. In Fig. 7 we show the F_2^n/F_2^p ratio calculated including the full range of nuclear variations considered in our fits. As in Fig. 6, the cross-hashed band illustrates the variation due to the choices made for the deuteron wave function and the off-shell corrections, while the hashed band shows in addition the uncertainty coming from the PDF errors. The arrow serves as a reminder that the bands at $x \gtrsim 0.8$ are an extrapolation unconstrained by data. Note that as a consequence of the positivity of the u and d quark distributions, F_2^n/F_2^p must be greater than $1/4$ for all values of x. (The PDF error band can exceed that limit because it was obtained with the Hessian technique, which assumes Gaussian errors also close to the limits of the PDF functional space.)

For comparison we also show in Fig. 7 the F_2^n/F_2^p ratio extracted assuming no nuclear corrections in deuterium. Above $x \approx 0.75$ the neutron structure function extracted under this assumption is significantly larger than the range allowed by our fits. (In fact, assuming $F_2^n = F_2^d - F_2^p$ implies a divergent experimental F_2^n/F_2^p ratio at $x = 1$, where F_2^p vanishes but

F_2^d remains finite.) The nuclear uncertainty in the F_2^n/F_2^p ratio in Fig. 7 is thus somewhat smaller at large x than would be the case if we had considered the entire range of possibilities for the nuclear effects, including the "no nuclear corrections" *ansatz*. Nonetheless, given the choice of the range of nuclear corrections discussed in Sec. II, the F_2^n/F_2^p ratio at $x \approx 1$ appears consistent with any value between $1/4$ and ≈ 0.7, covering all nonperturbative model predictions [48, 49].

A recent effort to extract the neutron structure function from inclusive deuterium data [51, 52] follows a complementary approach to that adopted here. Firstly, phenomenological fits to proton and deuteron structure functions are used to interpolate available data to a fixed value of Q^2. The data are then analyzed within the convolution framework, using a range of nuclear corrections selected from the literature [52]. The resulting size of uncertainties on the F_2^n/F_2^p ratio in Ref. [52] is smaller than but comparable to that in Fig. 7. However, the central value was found to decrease monotonically with x and show no sign of a plateau. This is in contrast to our findings, which suggest a possible plateau or even increase in F_2^n/F_2^p for $x \gtrsim 0.7 - 0.8$. An important difference between our analysis and that of Refs. [51, 52] is that our F_2^n/F_2^p ratio is determined from global fits of leading twist PDFs (which are constrained to be positive definite), utilizing a wide array of data, not restricted to hydrogen and deuterium DIS only. The data analyzed in [51, 52], on the other hand, are at the structure function level, including possible higher twist and other subleading $1/Q^2$ corrections, so that F_2^n/F_2^p is not constrained to lie above $1/4$.

It is worth reiterating that there is a wealth of data in the region up to $x = 0.98$ over a large range of photon virtualities, $7 < Q^2 < 31$ GeV^2, which most previous global fits have explicitly not utilized in order to avoid nonperturbative effects such as nucleon resonances, target mass and higher twist corrections. Our fits include a sizable fraction of these data, delineated by the cuts $Q^2 > 1.69$ GeV^2 and $W^2 > 3$ GeV^2, but still avoid most of the resonance region data, and are limited to $x \approx 0.8$ as indicated by the arrow in Fig. 7. These resonance region data are, however, included in the analysis of Ref. [51], and may account for some differences in the final results as compared to this work. Studies of the resonance region data using the standard nuclear corrections demonstrate agreement between the DIS data sets and averages over resonance region data [53–55], and future efforts will explore ways to incorporate the latter within a global PDF framework.

D. No-deuteron fits and the W asymmetry

One of our motivations for including the deuterium data in the global fit was to reduce the uncertainty on the d PDF in the large-x region. The results presented thus far indicate that variations in the choices for the nuclear models can be largely compensated by changes in the d PDF. The question thus naturally arises as to whether or not the addition of the deuterium data has helped reduce the error on the d PDF at all. This can be examined by comparing in Fig. 8 the results of two fits with and without the deuterium data; for the former, results are shown for our reference fit using nucleon smearing in the deuteron with the AV18 wave function and the mKP off-shell corrections.

Two things stand out in this figure. First, for a specific choice of the nuclear corrections, the d uncertainty is significantly reduced, as would be expected. Thus, if a method could be devised which would narrow the options for the choice of the nuclear models, then the deuterium data would provide the information that is needed to constrain the d-quark PDF. On the contrary, in the absence of constraints on the nuclear models, the systematic nuclear uncertainty is comparable to the PDF uncertainty in the no-deuteron fit. Secondly, the removal of the deuterium data results in a significant increase in the d/u ratio at *low* values of x, where the nuclear smearing and off-shell corrections to deuteron data are negligible. This was rather unexpected and suggests that the deuterium experiments are pulling against some combination of other data in this region. One might expect that in this region of low x nuclear shadowing corrections might be important; however, examination of various shadowing models suggests a correction of only a percent or so, insufficient to explain the shift in Fig. 8.

Inspection of the proton DIS data sets shows that the χ^2 improvement between the reference and no-deuteron fits is slight and is not confined to any specific region of x; this is true also for the lepton pair and jet data. However, the CDF W asymmetry data, shown in Fig. 9 (left panel), suggest a marked decrease in χ^2 of about 20 units at W rapidity $y_W < 1.9$. In contrast, for $y_W > 1.9$ the nuclear uncertainties become non-negligible, making it more difficult to quantify the χ^2 improvement of the no-deuteron fit, which is strongly dependent on the reference nuclear model. These observations can be understood by noting that the
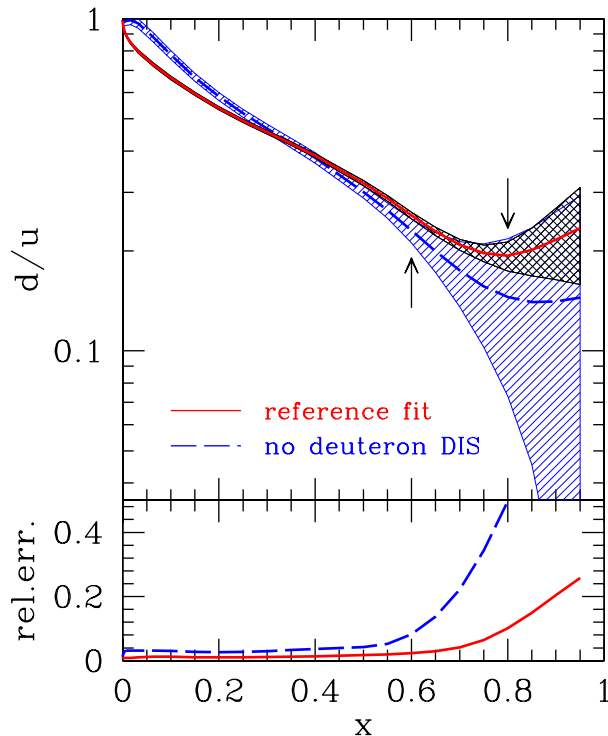
FIG. 8: d/u ratios extracted from our reference fit, using the nucleon smearing function in the deuteron with the AV18 wave function and the mKP (central) off-shell corrections. The solid curve utilizes all the data (with uncertainties given by the cross-hashed band); the dashed curve (with uncertainties given by the diagonal-hashed band) results from removing all the deuterium DIS data sets, avoiding the need for deuteron corrections. The PDF error bands correspond to $\Delta\chi = 1$. The arrows indicate the extrapolation region of each fit ($x > 0.6$ for the no-deuteron fit, and $x > 0.8$ for the full fit). The relative error of the two fits is shown in the bottom panel.

W asymmetry is approximately given by

$$A_W \approx \frac{(d/u)(x_2) - (d/u)(x_1)}{(d/u)(x_2) + (d/u)(x_1)}, \tag{23}$$

where $x_{1,2} = (M_{W^*}/\sqrt{s}) \exp(\pm y_W)$, and $M_{W^*}^2$ is the four-momentum squared of the virtual W boson. Equation (23) is a simple leading-order result in which the effects of the sea quarks are neglected and the antiquark distributions in the antiproton have been set equal to the quark distributions in the proton. It is clear that, at positive rapidity, increasing d/u at small x or decreasing d/u at large x results in an upward shift of A_W.

The interplay between y_W, x_1 and x_2 becomes clear from Fig. 10, which shows $x_{1,2}$ versus y_W at CDF kinematics (left panel), and the fitted the d/u ratios on a logarithmic x scale
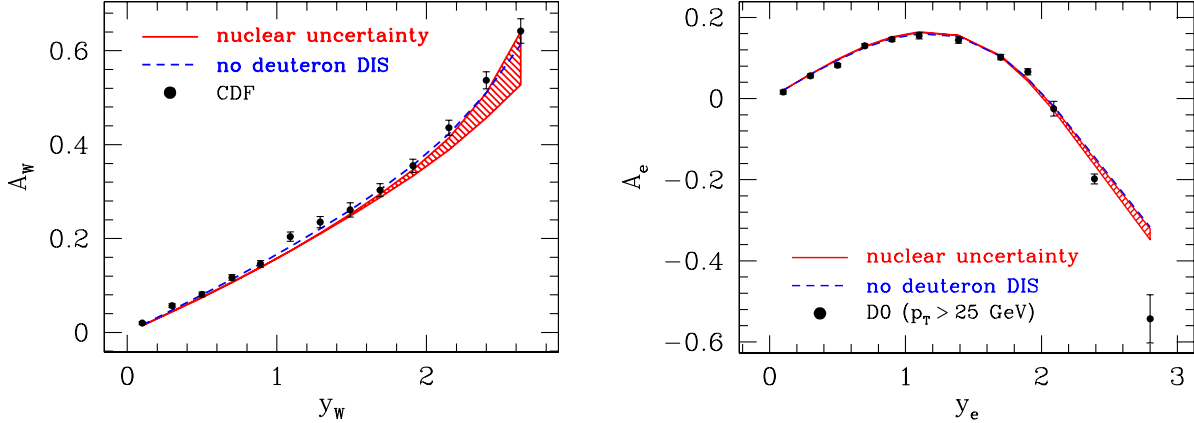
FIG. 9: *(Left)* The CDF W asymmetry data compared to the calculation using fits with deuteron data and nuclear corrections (shaded band) and the "no deuteron DIS" fit (dashed curve). *(Right)* The DØ W decay electron asymmetry data integrated over $p_T > 25$ GeV compared to the same fits.

(right panel) for the minimum and maximum nuclear corrections, and the no-deuteron fit. Data at $y_W > 2$ are sensitive to PDFs at $x_1 > 0.3$, where the nuclear correction uncertainties become increasingly large, and at $x_2 < 0.005$, where the difference between the full and no-deuteron fits becomes small and the d/u ratio is well constrained. Large-y_W data are thus mostly sensitive to large-x partons, and are affected by nuclear uncertainties. Data at $y_W < 2$ are sensitive to intermediate values of $x_{1,2} \in (0.01, 0.1)$, precisely where the deuteron and no-deuteron fits differ maximally. It is clear that the improvement in χ^2 at small y_W is entirely due to this region, where the deuteron DIS data and CDF W asymmetry data pull against each other.

The DØ collaboration data on the asymmetry A_e of the electrons originating from the W decay, integrated over electron transverse momenta $p_T > 25$ GeV, is shown in the right panel of Fig. 9: the small decrease in χ^2 observed at small lepton rapidity y_e is compensated by a small or large increase at large rapidity, depending on the reference nuclear correction. A similar behavior is observed in the DØ muon asymmetry data. Thus, in our fits, the lepton asymmetry data seem to pull only very slightly against the deuteron target DIS data. In this respect, one should note that due to the nature of the vector-axial vector decay of the W, the lepton asymmetry is less sensitive to the d/u ratio than is the case for the W asymmetry itself.
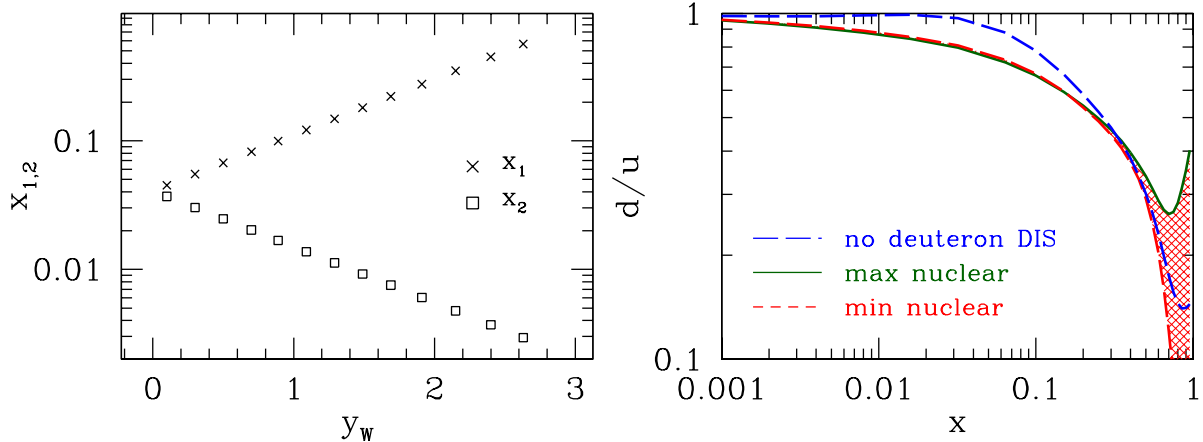
FIG. 10: *(Left)* Values of $x_{1,2}$ versus W rapidity y_W at CDF W kinematics. *(Right)* d/u ratios on a logarithmic x scale for the "no deuteron DIS" fit (long dashed), and for maximum (solid) and minimum (short-dashed) nuclear corrections.

In summary, these plots and the χ^2 inspection show that the CDF W asymmetry data and the DØ lepton asymmetry data seem collectively to prefer a somewhat larger d/u ratio than is favored by the deuterium DIS data in the region below $x \lesssim 0.2$. Moreover, as noted previously, at larger x the lepton asymmetry data prefer a somewhat larger ratio than the CDF W asymmetry. This unfortunately prevents them being used to constrain the nuclear corrections, to which they are mildly sensitive. The origin and possible resolutions of the tension between the W and lepton asymmetries, as well as that between these asymmetries and the deuteron data, is being actively discussed [2, 3, 57–59].

E. Parton luminosities at hadron colliders

To discuss the effects of the nuclear model dependence on different PDFs, the extremes of the d PDF are shown in Fig. 11 divided by the reference fit PDF, along with the corresponding u-quark and gluon PDFs. Even though the d PDF at large values of x varies by as much as $\approx 60\%$, the u PDF shows little variation. This is because the DIS and lepton pair data at large x are for the most part sensitive to the combination $4u + d$, and the d/u ratio is on the order of 0.1 in this region. Thus, the role played by the u PDF here is about 40 times more important that of the d PDF. Therefore, a small and anticorrelated shift in the u PDF can compensate for a large change in the d PDF.
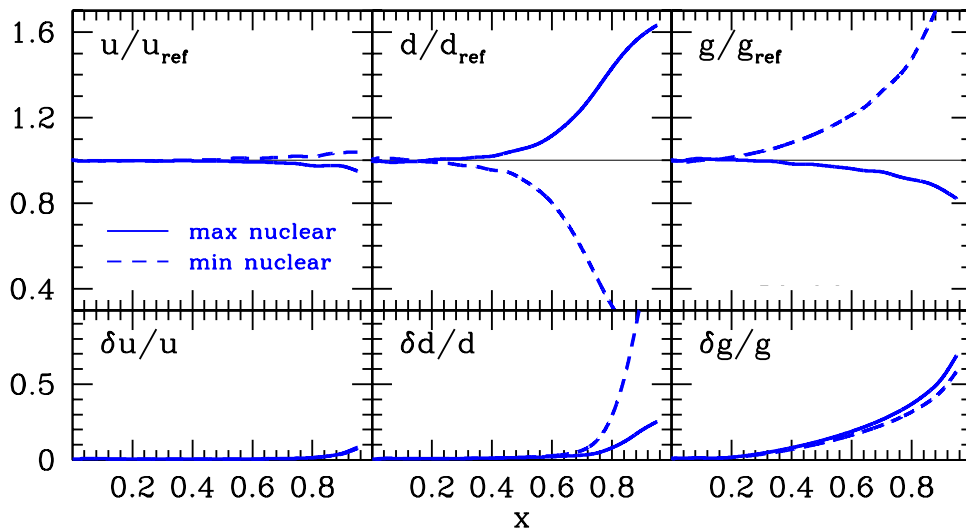
FIG. 11: The extremes of the variations of the u *(left panel)*, d *(middle panel)*, and gluon *(right panel)* PDFs, relative to reference PDFs extracted using the smearing function with the AV18 deuteron wave function and mKP (central) off-shell corrections (12).

The situation is somewhat different for the case of high-p_T jet production. This process receives contributions from qq, qg, and gg scattering subprocesses with the qq subprocesses dominating at large values of x for the target. Since the u PDF is already well constrained, a variation in the d PDF is compensated by a significant and anti-correlated shift in the gluon PDF. The sea quarks are largely unconstrained at large x, and follow the behavior of the gluon, that generates them radiatively; the only exception is the $\bar{d}$ quark, which seems to follow the d quark at $0.2 \lesssim x \lesssim 0.6$ and the gluon only at $x \gtrsim 0.6$.

The large nuclear uncertainty in the quark PDFs, and even more in the gluon PDF, which shows a significant variation at values of x as low as 0.4, have potentially profound implications for future collider experiments. As an illustration, we consider the parton luminosities

$$L_{ij} = \frac{1}{s(1+\delta_{ij})} \left[\int_{\hat{s}/s}^{1} \frac{dx}{x} f_i(x, \hat{s}) f_j\left(\frac{\hat{s}}{xs}, \hat{s}\right) + (i \leftrightarrow j) \right], \tag{24}$$

where s ($\hat{s}$) is the hadronic (partonic) center of mass energy squared, and $f_i(x, Q^2)$ is the PDF for a parton of flavor i (quark or gluon) at fractional momentum x and scale Q^2. In Fig. 12, the parton luminosities are plotted at $\sqrt{s} = 7$ TeV relevant to the current LHC runs. The gg luminosity controls the main channel for Higgs production, the gd luminosity
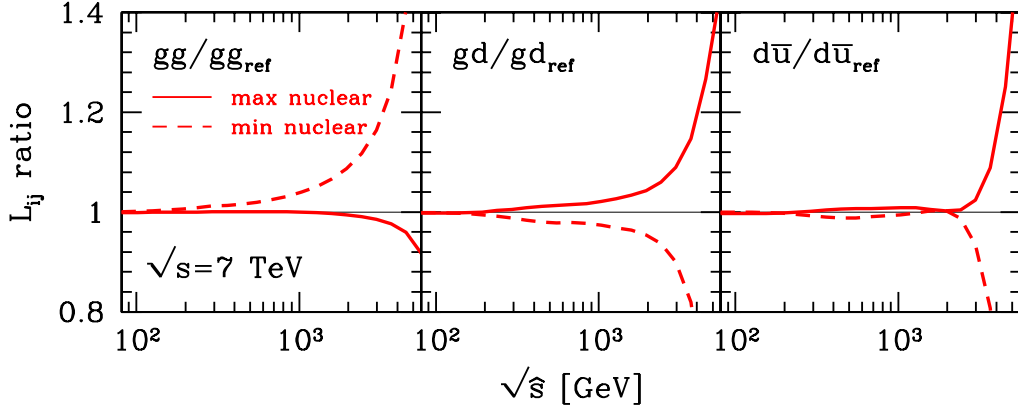
FIG. 12: Parton luminosities at $\sqrt{s} = 7$ TeV at the LHC. Shown are the extremes of the variations due to deuterium nucleon corrections of the *gg (left)*, *gd (middle)* and *d$\bar{u}$ (right)* luminosities relative to reference PDFs extracted using our default nucleon smearing function in the deuteron with the mKP (central) off-shell corrections (12).
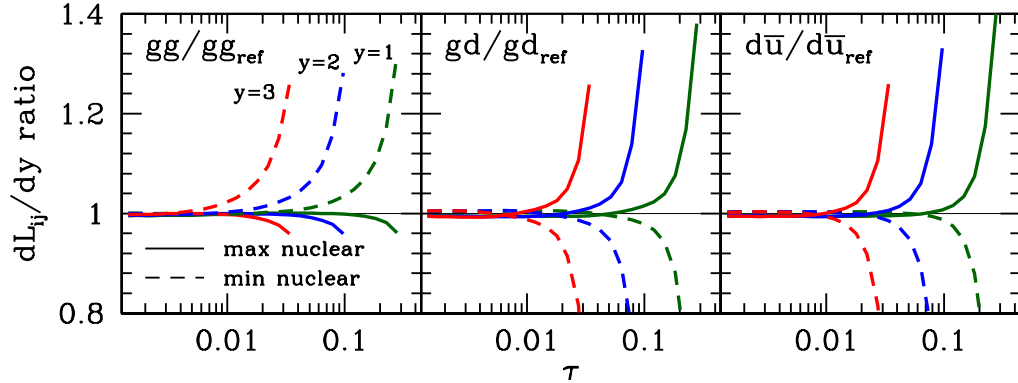

FIG. 13: Differential parton luminosities for *gg (left)*, *gd (middle)* and *d$\bar{u}$ (right)* at fixed rapidity $y = 1, 2$ and 3, as a function of $\tau = \sqrt{\hat{s}/s}$, illustrating the variations due to the choice of deuterium nucleon corrections.

is relevant for jet production, and the $d\bar{u}$ luminosity controls the "standard candle" cross section for W^- production. Figure 12, shows that the theoretical uncertainty induced by nuclear corrections extends to rather small scales $\sqrt{\hat{s}}$, and grows quickly above 5–10% as $\sqrt{\hat{s}}$ exceeds 1 TeV.

The luminosity ratios in Fig. 12 are relevant for the total cross section for producing an object with a mass equal to $\sqrt{\hat{s}}$. However, one can also investigate a specific region of x by

considering the production of an object of the same mass, but at a specified rapidity y (not to be confused with the momentum fraction y carried by a nucleon in the deuteron, as in Sec. II). The differential parton luminosity is then given by

$$\frac{dL_{ij}}{dy} = \frac{1}{s(1 + \delta_{ij})} \left[f_i(x_1, \hat{s}) f_j(x_2, \hat{s}) + (i \leftrightarrow j) \right],\tag{25}$$

where $x_{1,2} = \tau e^{\pm y}$, with $\tau = \sqrt{\hat{s}/s}$. The differential luminosities, normalized to calculations using our reference fit, are shown in Fig. 13 as a function of τ for three values of rapidity (since the ratios are largely independent of Q^2, these plots are also independent of s). The parton luminosities not plotted there show a qualitatively similar behavior. Going to larger rapidities increases the sensitivity to the large-x region for a given mass. Therefore, the nuclear corrections come into play for smaller masses as the rapidity is increased. For example, for W production at the Tevatron the nuclear uncertainty becomes relevant at rapidity larger than 2, as already observed in Sec. IV D.

V.   DISCUSSION

In the previous sections we have discussed in detail the fundamental problem with using deuterium DIS data to constrain the d-quark PDF at large x, namely, the deuterium data only constrain the *combination* of the d PDF *and* the model used to compute the nuclear corrections. Variations in the nuclear models are easily compensated by changes in the d distribution, while the u distribution is already well constrained by the hydrogen DIS data and other observables. It is also interesting to note that the resulting variations in the d PDF feed over to accompanying anticorrelated variations of the gluon PDF. In order to disentangle the d quark from the nuclear correction model, one either needs additional experimental observables which do not rely on nuclear targets, or experiments on nuclear targets for which it can be arranged that the results are less sensitive to nuclear corrections.

A.   Constraints on large-x d quarks

One approach to directly constrain d-quark PDFs, avoiding nuclear corrections altogether, would be to utilize data for νp DIS, which at large values of x is dominated by the d PDF. While such data exist [60], they were obtained using a hydrogen bubble chamber and are

statistically limited at large values of x. High statistics data for this process from new high intensity neutrino beam lines, such as NUMI at Fermilab, would provide a valuable constraint. This could possibly be realized in the near future, for example, if a hydrogen target were to be installed in the MINERνA experiment [61]. In addition, data on the ratio of νp to $\bar{\nu} p$ cross sections from a single experiment would provide direct sensitivity to d/u at large x, while allowing for a partial cancellation in the uncertainties associated with beam flux.

A similar source of information on the d PDF would be DIS data for charged current $e^+ p$ interactions [62]. These data were taken as part of the HERA experimental program, and will help constrain the d-quark PDF at small x, providing additional information concerning the observed tension between the deuterium DIS data and the CDF W asymmetry data. At large x they do not provide strong enough constraints due to limited statistics, even though a novel analysis is underway to extend their reach to the largest possible x [63]. Nevertheless, their inclusion in a full global fit should provide additional constraints on the d/u ratio.

Another observable sensitive to d/u is the Z rapidity distribution, since the weak coupling of the Z boson to the quarks makes it sensitive to a different combination of u and d quarks from the Drell-Yan lepton pair data. The cross section for Z-boson production involves a different linear combination of parton luminosities than either W production or lepton pair production, thereby offering yet another constraint on the d/u ratio. We intend, in a future study, to investigate this observable and include in our fits the available data, which currently have a limited statistical significance at large x. A better experimental understanding of the W asymmetry and W-lepton asymmetry data is also needed, since at large rapidity these data could help discriminate nuclear correction models. However, since they pull the d/u ratio in opposite directions, they cannot yet be used to this purpose.

At lower energies, a number of experiments have been proposed at Jefferson Lab which seek to reduce or eliminate the need for the nuclear corrections that limit current extractions of F_2^n, and the next 5 years promises to significantly improve the experimental situation with regards to the d PDF at $x \gtrsim 0.65$. This will be provided through both flavor sensitive probes in electron–proton scattering and electron scattering from *effective* neutron targets. Several of these experiments have already been approved for running at Jefferson Lab after the upgrade of the accelerator to 12 GeV, allowing for larger Q^2 and x to be probed for W^2 outside the nucleon resonance region.

One such method proposed for minimizing the nuclear uncertainties in F_2^n is the "MARATHON" [64] experiment, which aims to extract F_2^n/F_2^p from a measurement of the F_2 structure functions of tritium and ^{3}He. The use of these mirror nuclei allows for the cancellation of nuclear effects to the $\approx 1\%$ level [65], as well as many of the systematic uncertainties.

A complementary method which has recently been successfully implemented in the "BONUS" [66] experiment in Jefferson Lab Hall B is based on the spectator tagging technique. Here, low momentum protons tagged in the backward γd center-of-mass hemisphere in the scattering of electrons from a deuteron target ensures that the scattering took place off a nearly free neutron. The effects of final state interactions of the neutron debris with the spectator protons and nucleon off-shell corrections are minimized by restricting the protons to momenta to below 100 MeV/c and angles above 120°. Utilizing the measured momentum vector of the proton and the virtual photon, the initial momentum of the target neutron can be effectively determined, allowing for the kinematic correction of Fermi motion effects. The results from the BONUS experiment with a maximum beam energy of 5 GeV are limited to a maximum x of about 0.65; however, the power of the technique has been demonstrated and an extension to $x \approx 0.85$ and higher Q^2 has been approved for running at the 12 GeV energy [67].

Another novel, flavor-sensitive observable is provided by the parity-violating DIS asymmetry (resulting from the interference of γ^* and Z-boson exchange) on a hydrogen target [68], which yields a new combination of u and d PDFs at large x, and is free of any nuclear corrections. A 6 GeV run has been completed and subsequent runs are proposed for the 12 GeV era, over a range extending to $x \approx 0.8$ [69].

B. Constraints on large-x gluons

As discussed in Sec. IV, due to the interplay of deuteron DIS data and large-p_T jet data the gluon PDF is also very sensitive to nuclear corrections. Therefore these can also be constrained by considering independent observables sensitive to large x gluons. Two such observables are the longitudinal DIS structure function F_L, and the charm structure function F_2^c obtained by requiring at least one charmed particle in the final state of inclusive DIS.

The disadvantage of the F_L structure function is that the gluon PDF typically decreases

at large x much faster than the u and d quarks, which dominate this region. Therefore, in practice, the sensitivity of F_L to the gluons decreases fast as x approaches 1. The charm structure function is more directly related to the gluon distribution, but variations in the heavy-quark scheme used in the fit may in fact accommodate a number of possible gluon behaviors, as has been observed in recent fits of structure functions at HERA [70]. It would nonetheless be worthwhile to include F_L and F_2^c data in future fits to explore their power in constraining large-x gluons.

C. Constraints on nuclear corrections

The future free nucleon data discussed in Section V A open the possibility of no-deuteron fits with largely reduced d-quark PDF errors compared to that in Fig. 8, which uses currently available data sets. Having accurately determined the d-quark PDF at large x one can then confront the validity of various nuclear correction models directly. For instance, the free neutron F_2 structure functions can be calculated from the fitted PDFs, and used in the computation of the inclusive deuteron structure function. Any residual differences compared to data would then reflect directly the choice of nuclear model. Likewise, Drell-Yan pd data at *negative* rapidity, which may be reached in collider experiments such as at RHIC, could be used to further constrain the nuclear corrections in deuterium.

Global QCD fits, however, provide an even more powerful method of constraining the deuterium corrections, since they allow one to use a more diverse set of data, and to take full advantage of the statistical power of all the available data. For example, one could perform a global fit additionally including data sensitive to gluons, such as described in Section V B, and the deuteron DIS data themselves. For each given choice of nuclear corrections the fit would find PDFs, with very small PDF errors, that try to describe as well as possible both the deuteron data and the free nucleon data. A nuclear model that would, say, overcorrect the deuteron structure function would then produce PDFs poorly describing either data set. The phenomenologically viable nuclear corrections can then be selected among those that minimize the tensions between these data.

Such tests of nuclear models of the deuteron within global PDF fits will be complementary to direct experimental tests which will be made possible by the future data, and are an important prerequisite for an understanding of heavier nuclei.

VI. CONCLUSIONS

Deep inelastic scattering and lepton pair data taken on proton targets are generally sensitive the the combination $4u + d$ at large values of x. An additional linear combination is required in order to reliably separate the u and d PDFs. Traditionally, this role has been played by DIS data taken on a deuterium target. In this analysis we have investigated the uncertainties induced in the d PDF by variations in the choices made for modeling the deuterium nuclear corrections. We have shown that reasonable choices for the deuteron wave function and for modeling the off-shell effects result in large uncertainties in the d PDF as $x \rightarrow 1$. As expected, the use of deuterium data reduces the uncertainty on the d PDF for any given set of choices for the nuclear models. However, the totality of the induced uncertainties for all of the models is large.

The u PDF remains well determined despite the large uncertainties in the d PDF. This is due to the fact that the large-x DIS proton data and the large x_F lepton pair production data on both proton or deuteron targets are sensitive to $4u + d$, and at large values of x the ratio $d/u \sim \mathcal{O}(0.1)$ so that the role played by the d PDF there is down by a factor of ~ 40 relative to that of the u PDF. Thus, a small change in the u PDF can compensate a large change in the d PDF. On the other hand, the d and gluon PDFs are anticorrelated by the high-p_T jet data. The large uncertainties of the d PDF lead to large uncertainties of the gluon PDF which extend down to $x \approx 0.4$. This has potentially profound implications for future collider experiments.

This situation may be improved when data which are sensitive to the d/u ratio or gluons at large x, but which are *not* sensitive to nuclear corrections, become available. Several such experiments are planned and should take data in the near future. Inclusion of these data in global QCD fits will help constrain the phenomenologically viable range of nuclear correction models, thereby reducing the currently large uncertainties in the d-quark and gluon distributions.

34

---

[1] A. Accardi, M. E. Christy, C. E. Keppel, P. Monaghan, W. Melnitchouk, J. G. Morfin and J. F. Owens, Phys. Rev. D **81**, 034016 (2010).

[2] H. -L. Lai *et al.*, Phys. Rev. D **82**, 074024 (2010).

[3] A. D. Martin, W. J. Stirling, R. S. Thorne and G. Watt, Eur. Phys. J. C **63**, 189 (2009).

[4] R. D. Ball *et al.*, Nucl. Phys. **B838**, 136 (2010); R. D. Ball *et al.*, arXiv:1101.1300 [hep-ph].

[5] M. Gluck, P. Jimenez-Delgado and E. Reya, Eur. Phys. J. C **53**, 355 (2008); P. Jimenez-Delgado and E. Reya, Phys. Rev. D **79**, 074023 (2009).

[6] S. Alekhin, J. Blumlein, S. Klein and S. Moch, Phys. Rev. D **81**, 014032 (2010).

[7] F. D. Aaron *et al.*, JHEP **1001**, 109 (2010).

[8] S. A. Kulagin, G. Piller and W. Weise, Phys. Rev. C **50**, 1154 (1994); S. A. Kulagin, W. Melnitchouk, G. Piller and W. Weise, Phys. Rev. C **52**, 932 (1995).

[9] S. A. Kulagin and R. Petti, Nucl. Phys. **A765**, 126 (2006).

[10] Y. Kahn, W. Melnitchouk and S. A. Kulagin, Phys. Rev. C **79**, 035205 (2009).

[11] G. B. West, Phys. Lett. B **37**, 509 (1971).

[12] R. L. Jaffe, in *Relativistic Dynamics and Quark-Nuclear Physics*, M. B. Johnson and A. Pickleseimer editors (Wiley, New York, 1985).

[13] W. B. Atwood and G. B. West, Phys. Rev. D **7**, 773 (1973).

[14] J. S. Poucher *et al.*, Phys. Rev. Lett. **32**, 118 (1974).

[15] A. Bodek *et al.*, Phys. Rev. Lett. **30**, 1087 (1973); A. Bodek *et al.*, Phys. Rev. D **20**, 1471 (1979).

[16] P. V. Landshoff and J. C. Polkinghorne, Phys. Rev. D **18**, 153 (1978).

[17] L. L. Frankfurt and M. I. Strikman, Phys. Lett. B **76**, 333 (1978).

[18] A. C. Benvenuti *et al.*, Phys. Lett. B **189**, 483 (1987).

[19] A. C. Benvenuti *et al.*, Phys. Lett. B **237**, 599 (1990).

[20] J. J. Aubert *et al.*, Nucl. Phys. **B293**, 740 (1987).

[21] J. J. Aubert *et al.*, Phys. Lett. B **123**, 123 (1983).

[22] M. Arneodo *et al.*, Nucl. Phys. **B483**, 3 (1997).

[23] D. Allasia *et al.*, Phys. Lett. B **249**, 366 (1990).

[24] R. P. Bickerstaff and A. W. Thomas, J. Phys. G **15**, 1523 (1989).

[25] D. F. Geesaman, K. Saito and A. W. Thomas, Ann. Rev. Nucl. Part. Sci. **45**, 337 (1995).

[26] W. Melnitchouk, A. W. Schreiber and A. W. Thomas, Phys. Rev. D **49**, 1183 (1994).

[27] A. Accardi, J. W. Qiu and J. P. Vary, in preparation.

[28] R. B. Wiringa, V. G. J. Stoks and R. Schiavilla, Phys. Rev. C **51**, 38 (1995).

[29] R. Machleidt, Phys. Rev. C **63**, 024001 (2001).

[30] M. Lacombe, B. Loiseau, R. Vinh Mau, J. Cote, P. Pires and R. de Tourreil, Phys. Lett. B **101**, 139 (1981).

[31] F. Gross and A. Stadler, Phys. Rev. C **88**, 014005 (2008); *ibid.* C **82**, 034004 (2010).

[32] W. Melnitchouk, A. W. Schreiber and A. W. Thomas, Phys. Lett. B **335**, 11 (1994).

[33] L. L. Frankfurt and M. I. Strikman, Phys. Rep. **76**, 215 (1981).

[34] L. L. Frankfurt and M. I. Strikman, Nucl. Phys. **B250**, 143 (1985); Phys. Rep. **160**, 235 (1988).

[35] L. W. Whitlow *et al.*, Phys. Lett. B **282**, 475 (1992).

[36] U. K. Yang and A. Bodek, Phys. Rev. Lett. **82**, 2467 (1999).

[37] W. Melnitchouk, I. R. Afnan, F. R. P. Bissey and A. W. Thomas, Phys. Rev. Lett. **84**, 5455 (2000).

[38] A. Bodek, S. Dasu and S. E. Rock, in *Proceedings of the Fourth Conference on the Intersections between Particle and Nuclear Physics*, Tucson, Arizona, May 24-29, 1991 (SLAC-PUB-5598), `http://slac.stanford.edu/pubs/slacpubs/5500/slac-pub-5598.pdf`.

[39] J. Seely *et al.*, Phys. Rev. Lett. **103**, 202301 (2009).

[40] F. E. Close, R. L. Jaffe, R. G. Roberts and G. G. Ross, Phys. Rev. D **31**, 1004 (1985).

[41] G. Piller and W. Weise, Phys. Rept. **330**, 1 (2000).

[42] J. Kwiecinski and B. Badelek, Phys. Lett. B **208**, 508 (1988); B. Badelek and J. Kwiecinski, Nucl. Phys. **B370**, 278 (1992).

[43] W. Melnitchouk and A. W. Thomas, Phys. Rev. D **47**, 3783 (1993).

[44] W. Melnitchouk and A. W. Thomas, Phys. Rev. C **52**, 3373 (1995).

[45] G. Piller, W. Ratzka, W. Weise, Z. Phys. A **352**, 427 (1995).

[46] L. P. Kaptari and A. Y. Umnikov, Phys. Lett. B **272**, 359 (1991).

[47] L. Frankfurt, V. Guzey and M. Strikman, Phys. Rev. Lett. **91**, 202001 (2003).

[48] F. E. Close, Phys. Lett. B **43**, 422 (1973); G. R. Farrar and D. R. Jackson, Phys. Rev. Lett. **35**, 1416 (1975); N. Isgur, Phys. Rev. D **59**, 034013 (1999).

[49] W. Melnitchouk and A. W. Thomas, Phys. Lett. B **377**, 11 (1996).

[50] W. Melnitchouk and J. C. Peng, Phys. Lett. B **400**, 220 (1997).

[51] J. Arrington, F. Coester, R. J. Holt and T. S. Lee, J. Phys. G **36**, 025005 (2009).

[52] J. G. Rubin and J. Arrington, arXiv:1101.3506 [nucl-ex].

[53] P. E. Bosted and M. E. Christy, Phys. Rev. C **77**, 065206 (2008).

[54] S. P. Malace, Y. Kahn, W. Melnitchouk and C. E. Keppel, Phys. Rev. Lett. **104**, 102001 (2010).

[55]

[56] A. Accardi, arXiv:1101.5148 [hep-ph].

[57] R. S. Thorne, A. D. Martin, W. J. Stirling and G. Watt, PoS **DIS2010**, 052 (2010).

[58] R. D. Ball *et al.*, arXiv:1012.0836 [hep-ph].

[59] M. Guzzi *et al.*, arXiv:1101.0561 [hep-ph].

[60] G. T. Jones *et al.*, Z. Phys. C **44**, 379 (1989); G. T. Jones *et al.*, Z. Phys. C **62**, 575 (1994).

[61] D. Drakoulakos *et al.*, arXiv:hep-ex/0405002.

[62] S. Chekanov *et al.*, Eur. Phys. J. C **32**, 1 (2003).

[63] R. Ingbir, PoS **DIS2010**, 037 (2010).

[64] Jefferson Lab Experiment C12-10-103 [MARATHON], G. G. Petratos, J. Gomez, R. J. Holt and R. D. Ransome, spokespersons.

[65] I. R. Afnan *et al.*, Phys. Lett. B **493**, 36 (2000);
I. R. Afnan *et al.*, Phys. Rev. C **68**, 035201 (2003).

[66] Jefferson Lab Experiment E03-012 [BONUS], H. Fenker, C. E. Keppel, S. Kuhn and W. Melnitchouk, spokespersons,

[67] Jefferson Lab Experiment E12-10-102 [BONUS12], S. Bültmann, M. E. Christy, H. Fenker, K. Griffioen, C. E. Keppel, S. Kuhn and W. Melnitchouk, spokespersons.

[68] P. Souder, AIP Conf. Proc. **747**, 199 (2005).

[69] Jefferson Lab Experiment E12-10-007 [SoLID], P. Souder, spokesperson.

[70] A. Cooper-Sarkar, S. Glazov, K. Lipka, R. Placakyte and V. Radescu, DESY report H1-Prelim-10-143/ZEUS-Prel-10-019 (2010).